S. Vallipriyatharsini, A. Z. Bazeera, V. Chinnathambi & S. Rajasekar , J. Nonlinear Anal. Optim. Vol. 13(1) (2022), 25-38

Journal of Nonlinear Analysis and Optimization
Volume 13(1) (2022)
http://www.math.sci.nu.ac.th
ISSN : 1906-9685

J. Nonlinear Anal. Optim.

HOMOCLINIC TRANSITION TO CHAOS IN THE DUFFING OSCILLATOR DRIVEN BY PERIODIC PIECEWISE LINEAR FORCES

S. VALLIPRIYATHARSINI[1], A. Z. BAZEERA[1], V. CHINNATHAMBI*[1] AND S. RAJASEKAR[2]

[1] Department of Physics, Sadakathullah Appa College, Tirunelveli 627 011, Tamilnadu, India
[2] School of Physics, Bharathidasan University, Tiruchirapalli 620 024, Tamilnadu, India.

ABSTRACT. We have applied the Melnikov criterion to examine a homoclinic bifurcation and transition to chaos in the Duffing oscillator driven by different forms of periodic piecewise linear forces. The periodic piecewise linear forces considered are triangular, hat, trapezium, quadratic and rectangular types of forces. For all the forces, an analytical threshold condition for the homoclinic transition to chaos is derived using Melnikov method and Melnikov threshold curves are drawn in a parameter space. Using the Melnikov threshold curves, we have found a critical forcing amplitude f_c above which the system may behave chaotically. We have analyzed both analytically and numerically the homoclinic transition to chaos in the Duffing system with ϵ-parametric force also. The predictions from Melnikov method have been further verified numerically by integrating the governing equation and finding areas of chaotic behaviour.

KEYWORDS:Duffing oscillator, Melnikov criterion, Piecewise linear force, Homoclinic bifurcation, Chaos.
AMS Subject Classification: :37D45, 34C37, 34D10, 34A08, 37J20, 37C29.

1. Introduction

The forced Duffing oscillator is a seminal system for the study of chaotic dynamics and development of analytical and experimental techniques for nonlinear systems [1-5]. The problem of its nonlinear dynamics has attracted researchers from various fields of research across natural science and physics [6-8], mathematics [9,10], mechanical engineering [11-13] and electrical engineering [14-16]. Melnikov method is a powerful analytical tool to provide an approximate criterion for the occurrence of hetero/homoclinic chaos in a wide class of dynamical systems [17]. It is also

* *Corresponding author.*
Email address : veerchinnathambi@gmail.com.
Article history : Received 27 September 2020; Accepted 21 March 2022.

an effective approach to detect chaotic dynamics and to analyze near homoclinic motion with deterministic or random perturbation. Usually this method is applied explicitly to systems which possesses homoclinic orbits in multi-well potential like Duffing double-well or pendulum systems [18,19]. Recently, this method has been applied to certain nonlinear systems to predict the occurrence of horseshoe chaos [20-25].

In recent years there has been a great deal of interest on the study of effect of various periodic forces in certain linear and nonlinearly damped systems [26-30]. In the present paper, we study both analytically and numerically the effect of various periodic piecewise linear forces in the Duffing oscillator equation

$$\ddot{x} + \alpha\,\dot{x}\, - \omega_0^2 x + \beta x^3 = F(t), \tag{1.1}$$

where α is the damping coefficient, ω_0 is the natural frequency and β is the constant parameter which plays the role of nonlinear parameter. $F(t)$ is an external time dependent periodic driving force. Recently, Baber Ahmad [31] studied both analytically and numerically the stabilization of the pendulum motion with different forms of periodic piecewise linear forces. Our objective here is to explore the possibility of homoclinic transition to chaos in Eq.(1.1) using both analytical and numerical techniques. In the present analysis, we use Melnikov analytical method to study the influence of different forms of periodic piecewise linear forces.

The paper is organized in the following way. In Section 2, we obtain the Melnikov threshold condition for the transverse intersections of homoclinic orbits for the system (1.1) separately for each of the above periodic piecewise linear forces. In Section 3, we analyze the homoclinic transition to chaos by plotting the Melnikov threshold curves in $(f-\omega)$ parameter plane where f and ω are the amplitude and frequency of the external periodic forces and numerically measuring the time τ_M elapsed between two successive transverse intersections for all the forces. We verify the analytical prediction with the numerically calculated critical values of f at which the transverse intersections of stable and unstable manifolds of the saddle occur. The Melnikov threshold value is also compared with the onset of asymptotic chaos wherever possible. In Section 4 we analyze the homoclinic transition to chaos in the system (1.1) driven by an ϵ-parametric control force. Finally Section 5 contains the concluding remarks.

2. Calculation of Melnikov function

We consider the perturbed Duffing equation with periodic piecewise linear forces in the form

$$\dot{x} = y \tag{2.1a}$$

$$\dot{y} = \omega_0^2 x - \beta x^3 + \epsilon[-\alpha\,\dot{x}\, + F(t)] \tag{2.1b}$$

where ϵ is a small parameter. The periodic piecewise linear forces of our interest are triangular, hat, trapezium, quadratic and rectangular types of forces. Figure 1 depicts the different forms of periodic piecewise linear forces.

The unperturbed system ($\epsilon = 0$) with the potential and Hamiltonian functions are given by

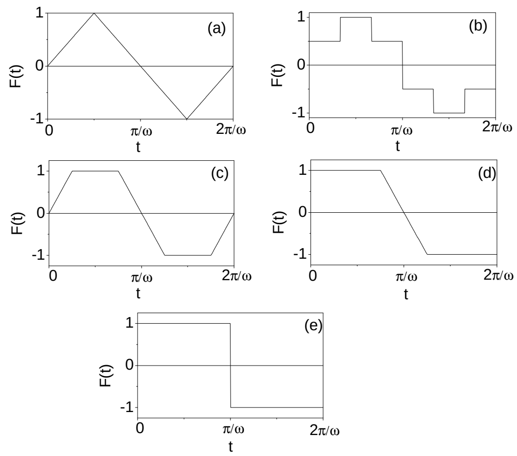

FIGURE 1. Form of various periodic piecewise linear forces (a) Triangular wave (b) Hat wave (c) Trapezium wave (d) Quadratic wave and (e) Rectangular wave. For all the forces period is $2\pi/\omega$, $\omega = 1$ and amplitude f is 1.0.

$$V(x) = -\frac{1}{2}\,\omega_0^2 x^2 + \frac{1}{4}\,\beta x^4. \tag{2.2}$$

$$H(x, y) = \frac{1}{2}\,y^2 - \frac{1}{2}\,\omega_0^2 x^2 + \frac{1}{4}\,\beta x^4. \tag{2.3}$$

Depending on the set of parameters, it can be considered at least three physically interesting situations where the potential is single-well, double-well and double hump-well. Throughout this paper, our analysis is of the double-well case. The unperturbed system has three fixed points. The origin is a saddle $(x^*, y^*) = (0, 0)$ and the other two fixed points are elliptic $(x^*, y^*) = (\pm\sqrt{\omega_0^2/\beta}, 0)$. The saddle point is connected to itself by two homoclinic orbits. The two homoclinic orbits connecting the saddle to itself are given by

$$W^{\pm}(x_h(\tau), y_h(\tau)) = \left(\pm\sqrt{\frac{2\,\omega_0^2}{\beta}}\ \mathrm{sech}\sqrt{\omega_0^2}\tau, \mp\omega_0^2\sqrt{\frac{2}{\beta}}\ \mathrm{sech}\sqrt{\omega_0^2}\tau\ \tanh\sqrt{\omega_0^2}\tau\right) \tag{2.4}$$

where $\tau = t - t_0$. The phase space motion of Eq.(2.1) is illustrated in Fig.2. The homoclinic orbits are indicated in it.

The Melnikov theory [9,12,17,32] allows us to calculate the Melnikov function $M(t_0)$ for a class of perturbed system for which homoclinic or heteroclinic orbit is known either analytically or numerically. $M(t_0)$ is proportional to the distance between the stable manifold (W_s) and unstable manifold (W_u) of a saddle. When the stable and unstable manifolds are separated then the sign of $M(t_0)$ always remain same. $M(t_0)$ oscillates when (W_s) and (W_u) intersects transversely (*horseshoe dynamics*). A zero of $M(t_0)$ corresponds to tangential intersections. The occurrence of transverse intersections implies that the Poincaré map of the system has the so called *horseshoe chaos*.

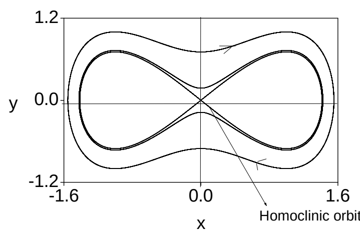

FIGURE 2. Phase trajectories of the unperturbed Duffing oscillator. The analytical expression for the homoclinic orbits is given by Eq.(2.4).

For Eq.(2.1), the Melnikov function is

$$M^{\pm}(t_0) = \int_{-\infty}^{+\infty} y_h \left[-\alpha\, y_h + F(\tau + t_0)\right]\, d\tau \tag{2.5}$$

In the following, we calculate the Melnikov function for the system (Eq.(2.1)) with different forms periodic piecewise linear forces. The period of all the forces are set to $T = 2\pi/\omega$.

2.1. **Triangular Type Force.** For the system (2.1) driven by Triangular type force,

$$F(t) = \begin{cases} \frac{4ft}{T}, & 0 \le t < \frac{T}{4} \\ -\frac{4ft}{T} + 2f, & \frac{T}{4} \le t < \frac{3T}{4} \\ \frac{4ft}{T} - 4f, & \frac{3T}{4} \le t < T, \end{cases} \tag{2.6}$$

where t is taken as mod $(2\pi/\omega)$. Its Fourier series is

$$F(t) = \frac{8f}{\pi^2} \sum_{n=1}^{\infty} \frac{(-1)^{(n+1)} \sin(2n-1)\omega t}{(2n-1)^2}. \tag{2.7}$$

Using Eq.(2.7), the Melnikov function is worked out as

$$M^{\pm}(t_0) \;=\; A \pm f \sum_{n=1}^{\infty} B_n\, \cos(2n-1)\omega t_0 \tag{2.8a}$$

where,

$$A \;=\; -\frac{4}{3}\frac{\alpha(\omega_0^2)^{3/2}}{\beta}, \tag{2.8b}$$

$$B_n \;=\; \frac{8\sqrt{2}\omega}{\pi\sqrt{\beta}}\, \frac{(-1)^{n+1}}{(2n-1)}\, \mathrm{sech}\left[\frac{(2n-1)\pi\omega}{2\sqrt{\omega_0^2}}\right] \tag{2.8c}$$

2.2. **Hat Type Force.** For the system (2.1) driven by Hat type force,

$$F(t) = \begin{cases} \frac{f}{2}, & 0 \le t < \frac{T}{6} \\ f, & \frac{T}{6} \le t < \frac{T}{3} \\ \frac{f}{2}, & \frac{T}{3} \le t < \frac{T}{2} \\ \frac{-f}{2}, & \frac{T}{2} \le t < \frac{2T}{3} \\ -f, & \frac{2T}{3} \le t < \frac{5T}{6} \\ \frac{-f}{2}, & \frac{5T}{6} \le t < T \end{cases} \tag{2.9}$$

Its Fourier series is

$$F(t) = \sum_{n=1}^{\infty} \frac{1}{n\pi} \left(1 - \cos n\pi + 2\cos\frac{n\pi}{3}\right) \sin n\omega t \tag{2.10}$$

Using Eq.(2.10), the Melnikov function is worked out to be

$$\begin{aligned} M^{\pm}(t_0) \quad = \quad & A \mp f \sum_{n=1}^{\infty} C_n \, n \cos n\omega t_0 \pm f \sum_{n=1}^{\infty} D_n \left[\cos(n\pi + n\omega t_0) - \cos(n\pi - n\omega t_0)\right] \\ & \mp f \sum_{n=1}^{\infty} E_n \left[\cos(n\pi/3 + n\omega t_0) - \cos(n\pi/3 - n\omega t_0)\right] \end{aligned} \tag{2.11a}$$

where,

$$C_n = \sqrt{2/\beta}\, \omega \text{ sech}\left[\frac{n\pi\omega}{2\sqrt{\omega_0^2}}\right] \tag{2.11b}$$

$$D_n = \frac{1}{\sqrt{2\beta}}\, \omega \text{ sech}\left[\frac{n\pi\omega}{2\sqrt{\omega_0^2}}\right] \tag{2.11c}$$

$$E_n = 2\sqrt{2\beta}\, \omega \text{ sech}\left[\frac{n\pi\omega}{2\sqrt{\omega_0^2}}\right] \tag{2.11d}$$

2.3. **Trapezium Type Force.** The mathematical representation for the Trapezium type force is

$$F(t) = \begin{cases} \frac{8ft}{T}, & 0 \le t < \frac{T}{8} \\ f, & \frac{T}{8} \le t < \frac{3T}{8} \\ \frac{8f}{T}(\frac{T}{2} - t), & \frac{3T}{8} \le t < \frac{5T}{8} \\ -f, & \frac{5T}{8} \le t < \frac{7T}{8} \\ \frac{8f(t-T)}{T}, & \frac{7T}{8} \le t < T. \end{cases} \tag{2.12}$$

Its Fourier series is

$$F(t) = \frac{16}{\pi^2} \sum_{n=0}^{\infty} \frac{1}{n^2} \sin\left(\frac{n\pi}{4}\right) \sin n\omega t \tag{2.13}$$

Using Eq.(2.13), the Melnikov function is worked out to be

$$M^{\pm}(t_0) = A \mp f \sum_{n=1}^{\infty} F_n \left[\sin(n\pi/4 + n\omega t_0) - \sin(n\pi/4 - n\omega t_0)\right] \tag{2.14a}$$

where,

$$F_n = \frac{8\sqrt{2/\beta}\,\omega}{\pi} \frac{1}{n} \text{ sech}\left[\frac{n\pi\omega}{2\sqrt{\omega_0^2}}\right]. \tag{2.14b}$$

2.4. **Quadratic Type Force.** The mathematical expresssion for the Quadratic type force is

$$F(t) = \begin{cases} f, & 0 \le t < \frac{3T}{8} \\ \frac{8f}{T}(\frac{T}{2} - t), & \frac{3T}{8} \le t < \frac{5T}{8} \\ -f, & \frac{5T}{8} \le t < T. \end{cases} \tag{2.15}$$

Its Fourier series is

$$F(t) = \sum_{n=0}^{\infty} \left(\frac{2f}{n\pi} + \frac{8f}{n^2\pi^2} \sin\left(\frac{n\pi}{4}\right)\right) \sin n\omega t \tag{2.16}$$

Using Eq.(2.16), the Melnikov function is worked out to be

$$\begin{aligned} M^{\pm}(t_0) &= A \mp f \sum_{n=1}^{\infty} G_n \cos n\omega t_0 \mp \\ & \quad f \sum_{n=1}^{\infty} H_n \left[\sin(n\pi/4 + n\omega t_0) - \sin(n\pi/4 - n\omega t_0)\right] \qquad (2.17a) \end{aligned}$$

where,

$$G_n = 2\sqrt{2/\beta}\,\omega\ \mathrm{sech}\left[\frac{n\pi\omega}{2\sqrt{\omega_0^2}}\right] \qquad (2.17b)$$

$$H_n = \frac{4\sqrt{2/\beta}\,\omega}{\pi}\ \frac{1}{n}\ \mathrm{sech}\left[\frac{n\pi\omega}{2\sqrt{\omega_0^2}}\right]. \qquad (2.17c)$$

2.5. **Rectangular Type Force.** The mathematical representation for the Rectangular type force is

$$F(t) = \begin{cases} f, & 0 \le t < \frac{T}{2} \\ -f, & \frac{T}{2} \le t < T. \end{cases} \qquad (2.18)$$

Its Fourier series is

$$F(t) = \frac{4f}{\pi} \sum_{n=0}^{\infty} \frac{1}{(2n-1)}\ \sin(2n-1)\omega t \qquad (2.19)$$

Using Eq.(2.19), the Melnikov function is worked out to be

$$M^{\pm}(t_0) = A \mp f \sum_{n=0}^{\infty} I_n\ \cos(2n-1)\omega t_0 \qquad (2.20a)$$

where,

$$I_n = 4\sqrt{2/\beta}\,\omega\ \mathrm{sech}\left(\frac{(2n-1)\pi\omega}{2\sqrt{\omega_0^2}}\right). \qquad (2.20b)$$

From Eqs.(2.8), (2.11), (2.14), (2.17) and (2.20) we can obtain the condition for transverse intersections of stable manifolds ($W_s^{\pm}$) and unstable manifolds ($W_u^{\pm}$), that is, $M^{\pm}(t_0)$ to change sign at some t_0.

3. Homoclinic Transition to Chaos

In this section we analyze the occurrence of homoclinic transition to chaos in the system (2.1) driven by different forms of periodic piecewise forces. For our study we fix the values of the parameters in Eq.(2.1) as $\alpha = 0.5, \beta = 1.0, \omega_0^2 = 1.0$ and $\omega = 1.0$. We consider sufficiently large number of terms, say, 100 terms in the summation of equation for $M(t_0)$. Figure 3 shows the plot of f_M versus n, the number of terms in the summation (Eq.(2.8)) for the triangular type force. f_M converses to a constant value with increase in n. For $n > 5$, the variation of f_M is negligible. Similar result is found for other types of periodic piecewise linear forces also. Hence in our numerical calculation we fix $n = 50$. First we analyze the occurrence of homoclinic transition to chaos numerically by measuring the time τ_M elapsed between two successive change in the sign of $M(t_0)$. For a fixed value of f, t_0 is varied from 0 to $200T$, where $T = 2\pi/\omega$ is the period of the driving force. If the sign of $M(t_0)$ remains the same in this time interval then there is no zero of $M(t_0)$ and τ_M is assumed to infinity. τ_M can be determined from the Eqs.

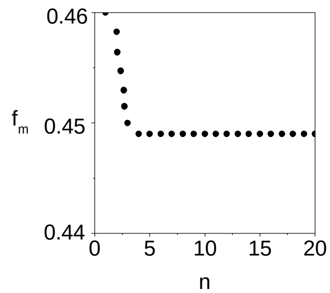

FIGURE 3. f_{M} versus n, the number of terms in the summation in Eq.(2.8a), for $\alpha = 0.5$, $\beta = 1.0$, $\omega_0^2 = 1.0$ and $\omega = 1$, when the system (2.1) is driven by the triangular type force. Variation in f_M converges to a constant value with increase in n.

(2.8),(2.11),(2.14),(2.17) and (2.20) for triangular, hat, trapezium, quadratic and rectangular types of forces. τ_M is calculated for a range of amplitude of the driving force. The value of f at which first intersection time of $M(t_0)$ changes sign and thereby giving finite τ_M is the Melnikov threshold value for homoclinic transition to chaos. Figure 4 shows the variation of $1/\tau_M$ versus f for the system (2.1) driven by different forms of periodic piecewise linear forces. Continuous curve represents the inverse of first intersection time $(1/\tau_{M^+})$ of stable and unstable branches of homoclinic orbits W^+. Dashed curve corresponds to the orbits of W^-. Homoclinic transition to chaos does not occur when $1/\tau_M$ is zero and it occurs in the region when $1/\tau_M > 0$.

In Fig.4(a), when the system (2.1) driven by triangular type force, both $1/\tau_{M^+}$ and $1/\tau_{M^-}$ are zero (that is $1/\tau_{M^\pm}$ are infinity) in the interval $0 < f < 0.45707$. This implies that homoclinic transition to chaos does not occur for $f < f_M^\pm = 0.45707$. For $f > f_M^\pm$=0.45707, both $M^+(t_0)$ and $M^-(t_0)$ oscillate and hence $1/\tau_M$ are nonzero. This implies that homoclinic transition to chaos is possible in this region. The Melnikov threshold values of the other types of periodic piecewise linear forces, namely, hat, trapezium, quadratic and rectangular types of forces are $f_M^\pm = 0.29206, 0.31680, 0.42605$ and 0.27948. From these values, it is observed that, among the five forces, f_M is maximum for the triangular type force and is minimum for the rectangular type force. Thus the onset of homoclinic transition to chaos can be either delayed or advanced by an appropriate choice of periodic piecewise linear forces.

Then we analyze the occurrence of homoclinic transition to chaos by plotting the threshold curves in the $(f - \omega)$ parameters plane also. The threshold curves for homoclinic transition to chaos in the (f, ω) plane for the different forms of periodic piecewise linear forces are shown in Fig.5. In the parameter region below the threshold curve no transverse intersection of stable and unstable manifolds of saddle occurs and above the threshold curve the transverse intersection of stable and unstable manifolds of the saddle occur. Just above the Melnikov threshold curve onset of cross-well chaos is expected. This figure clearly illustrates the effect of various periodic piecewise forces.

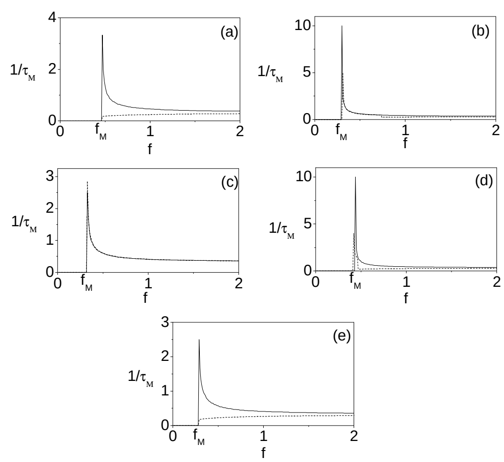

FIGURE 4. Variation of $1/\tau_M$ versus f for the system (2.1) driven by (a) triangular, (b) hat, (c) trapezium, (d) quadratic and (e) rectangular types of forces. The values of the other parameters are $\alpha = 0.5$, $\beta = 1$, $\omega_0^2 = 1$ and $\omega = 1$. Solid curve is for positive sign in $M(t_0)$ and dashed curve is for negative sign in $M(t_0)$.

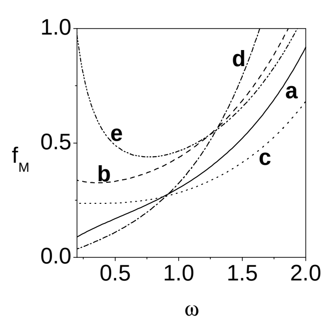

FIGURE 5. Melnikov threshold curves for horseshoe chaos in the $(f-\omega)$ plane for the system (2.1) driven by the forces (a) triangular, (b) hat, (c) trapezium, (d) quadratic and (e) rectangular types of forces. The values of the other parameters in Eq.(2.1) are $\alpha = 0.5$, $\beta = 1$ and $\omega_0^2 = 1$.

We have verified the analytical prediction by direct simulation of the system (1.1). In Fig.6 we plotted the orbits of the saddle for two values of the forces - one for $f < f_M$ and another for $f > f_M$. For clarity, only part of the manifolds are shown. The unstable manifolds are obtained by numerically integrating the Eq.(1.1) by the fourth-order Runge-Kutta method in the forward time for a set of 900 initial conditions chosen around the perturbed saddle point. The stable manifolds are obtained by integrating the the Eq.(1.1) in reverse time. In the left side subplots (Figs.6a,6c,6e,6g and 6i), $f < f_M$ the stable and unstable manifolds are well separated. That is homoclinic transition to chaos does not occurs in this region. In the right side subplots (Figs.6b,6d,6f,6h and 6j) for $f > f_M$, we can clearly

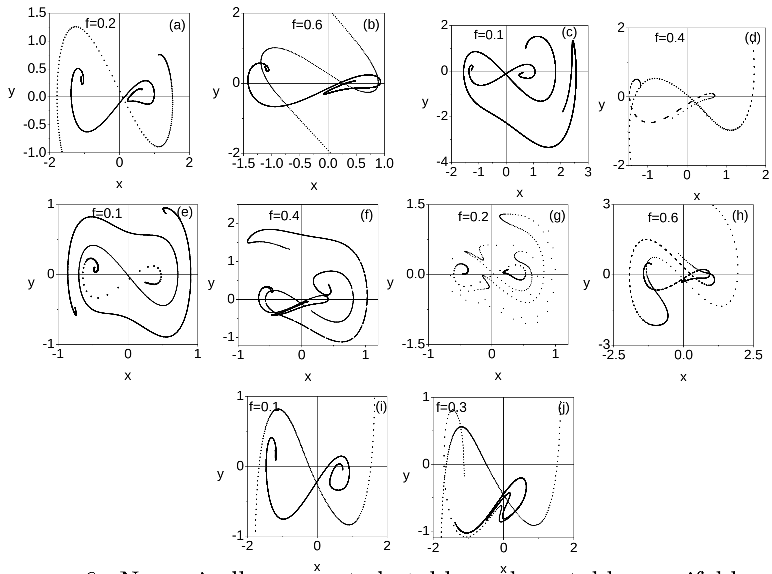

Figure 6. Numerically computed stable and unstable manifolds of the saddle fixed point of the system (2.1). The system is driven by (a-b) triangular, (c-d) hat, (e-f) trapezium, (g-h) quadratic and (i-j) rectangular types of forces. The values of the other parameters are $\alpha = 0.5$, $\beta = 1$, $\omega_0^2 = 1$ and $\omega = 1$. Left side subplots (Figs.6a,6c,6e,6g and 6i) are for $f < f_M$ while the right side subplots (Figs.6b,6d,6f,6h and 6j) are for $f > f_M$.

notice the transverse intersections of orbits at certain places. That is homoclinic transition to chaos is possible in this region.

4. Homoclinic Transition to Chaos due to an ϵ-Parametric Control Force

In the previous section, all the above results can be considered as nonparametric control force. In this section, an ϵ-parametric control force is defined one of the periodic piecewise linear force. This ϵ-parametric force with $0 < \epsilon < 1$ is given by (similar to quadratic type force (Eq.(2.15)),

$$F(t) = \begin{cases} f, & 0 \le t < \frac{1-\epsilon}{2}\,T \\ \frac{f}{\epsilon}(\frac{-2}{T}t + 1), & \frac{1-\epsilon}{2}T \le t < \frac{1+\epsilon}{2}\,T \\ -f, & \frac{1+\epsilon}{2}T \le t < T. \end{cases} \tag{4.1}$$

and is illustrated in Fig.7 with different values of ϵ, namely, $\epsilon = 0.17, 0.5, 0.7$ and 0.9. Its Fourier series is

$$F(t) = \sum_{n=1}^{\infty} \left(\frac{2f}{n\pi} + \frac{2f}{\epsilon\, n^2\pi^2}\ \sin(\epsilon n\pi) \right)\ \sin n\omega t \tag{4.2}$$

Using Eq.(4.2), the Melnikov function is worked out to be

$$M^{\pm}(t_0) \;=\; A \mp f \sum_{n=1}^{\infty} J_n \cos n\omega t_0\ \mp$$

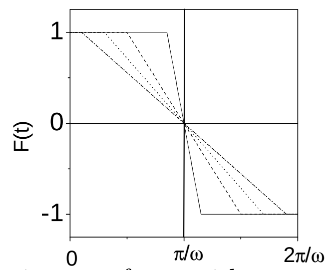

FIGURE 7. Form of Quadratic type force with $\epsilon = 0.17$(solid curve), $\epsilon = 0.5$(dashed curve), $\epsilon = 0.7$(dotted curve) and $\epsilon = 0.9$(dashed dot curve).

$$f \sum_{n=1}^{\infty} K_n \left[\sin(\epsilon n\pi + n\omega t_0) - \sin(\epsilon n\pi - n\omega t_0)\right] \tag{4.3a}$$

where,

$$J_n = 2\sqrt{2/\beta}\,\omega \operatorname{sech}\left[\frac{n\pi\omega}{2\sqrt{\omega_0^2}}\right] \tag{4.3b}$$

$$K_n = \frac{\sqrt{2/\beta}}{\epsilon n\pi}\,\omega \operatorname{sech}\left[\frac{n\pi\omega}{2\sqrt{\omega_0^2}}\right]. \tag{4.3c}$$

and the value of A is given in Eq.(2.8(b)). The occurrence of homoclinic transition

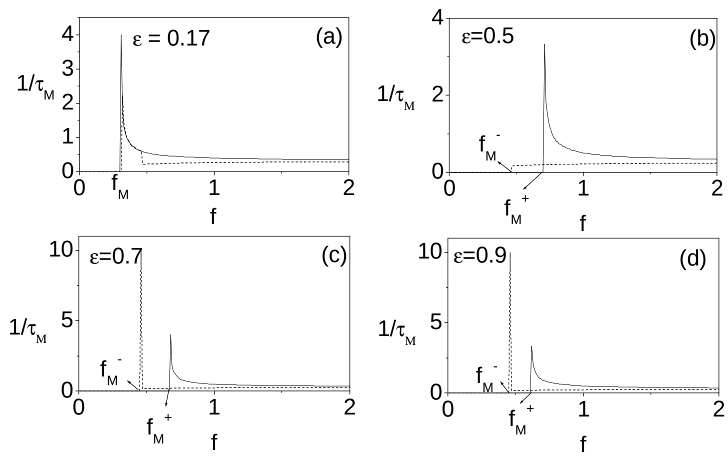

FIGURE 8. Variation of $1/\tau_M$ versus f for the system (2.1) driven by the $\epsilon-$ parametric force for four values of ϵ, namely, $\epsilon = 0.17, 0.5, 0.7, 0.9$. The values of the other parameters are $\alpha = 0.5$, $\beta = 1$, $\omega_0^2 = 1$ and $\omega = 1$. Solid curve is for positive sign in $M(t_0)$ and dashed curve is for negative sign in $M(t_0)$.

to chaos can be studied numerically measuring the time τ_M elapsed between two successive transverse intersections. τ_M can be determined from Eq.(4.3). Figure 8 shows the variation of $1/\tau_{M^\pm}$ versus f for four values of ϵ, namely, $\epsilon = 0.17, 0.5, 0.7$ and 0.9. Continuous curve represents the inverse of first intersection time $(1/\tau_M)$ of stable and unstable branches of homoclinic orbits W^+. Dashed curve corresponds to the orbits of W^-. Homoclinic transition to chaos does not occur when $1/\tau$ is zero and it occurs in the region $1/\tau > 0$. In Fig.8(a), for $\epsilon = 0.17$, both $1/\tau_{M^+}$ and $1/\tau_{M^-}$ are zero in the interval $0 < f < 0.29736$. This implies that homoclinic transition to chaos does not occur for $f < f_M^\pm = 0.29736$. For $f > f_M^\pm = 0.29736$, both $M^+(t_0)$ and $M^-(t_0)$ oscillate and hence $1/\tau_{M^\pm}$ are nonzero. This implies that homoclinic transition to chaos is possible in this region. For $\epsilon = 0.5$, $1/\tau_{M^+}$ and $1/\tau_{M^-}$ are zero for $f < f_M^+ = 0.70023$ and $f < f_M^- = 0.46077$ respectively. For f values in the interval $f_M^- < f < f_M^+$, $M_-(t_0)$ alone oscillate which implies that the homoclinic transition to chaos can take place only in the region $x < 0$. For $f \geq f^+$, homoclinic transition can occur in both regions $x < 0$ and $x > 0$. The Melnikov threshold values for $\epsilon = 0.7$ we find $f_M^+ = 0.66667$ and $f_M^- = 0.44897$; for $\epsilon = 0.9$ $f_M^+ = 0.60714$ and $f_M^- = 0.45068$.

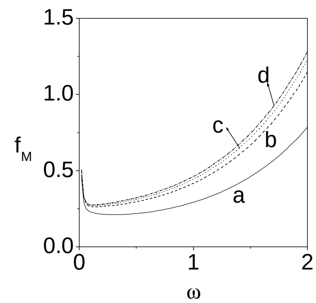

FIGURE 9. Melnikov threshold curves for horseshoe chaos in the $(f - \omega)$ plane for the system (2.1) driven by an $\epsilon-$ parametric force for four values of ϵ, namely, (a) $\epsilon = 0.17$, (b) $\epsilon = 0.5$, (c) $\epsilon = 0.7$ and (d) $\epsilon = 0.9$. The values of the other parameters in Eq.(2.1) are $\alpha = 0.5$, $\beta = 1$ and $\omega_0^2 = 1$.

The threshold curve for homoclinic transition to chaos in the (f, ω) plane for four values of ϵ, namely, $\epsilon = 0.17, 0.5, 0.7, 0.9$ is shown in Fig.9. Above the threshold curve, the system can transit to chaotic motions and below the threshold curve the system shows periodic behaviour. The results are also verified in Fig.10. The numerically computed W^s and W^u of the sadddle in the Poincar*é* map for $\epsilon = 0.5$ is shown in Fig.10. Transverse intersections of stable and unstable branches of both the homoclinic orbits are seen in Fig.10(c) for $f = 0.8$ (which is above the threshold value $f_M^+ = 0.70023$). For $\epsilon = 0.6$ (which is in between f_M^- and f_M^+), we see the transverse intersections of W_s^- and W_s^+ orbits alone at two places, which is clearly evident in Fig.10(b). The stable and unstable orbits are well separated in Fig.10(a) for $f = 0.2$ (which is below f_M^-). Homoclinic transition to chaos does not occur in this region. Similarly, we can verified the analytical results for other values of ϵ, namely, $\epsilon = 0.17, 0.7$ and 0.9. For different values of ϵ, the Melnikov threshold values of the system (2.1) driven by ϵ-parametric force is given in table 1. From table 1 we observed that the Melnikov threshold value of rectangular force falls

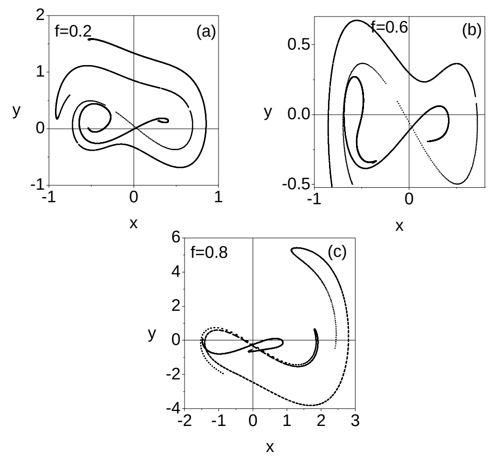

FIGURE 10. Numerically computed stable and unstable manifolds of the saddle fixed point of the system (2.1) driven by an $\epsilon-$ parametric force for three values of f with $\epsilon = 0.5$. The values of the other parameters are $\alpha = 0.5$, $\beta = 1$, $\omega_0^2 = 1$ and $\omega = 1$.

between $\epsilon = 0.2$ and $\epsilon = 0.1$. More clearly the parametric force with $\epsilon = 0.17...$ gives the Melnikov threshold value $(f_M^{\pm})$ almost equals with rectangular force. For $\epsilon \to 0$, ϵ-parametric force becomes quadratic type force.

TABLE 1. Melnikov threshold values of the system (2.1) with $\epsilon-$ parametric force for few values of ϵ with $\alpha = 0.5$, $\omega_0^2 = 1$, $\beta = 1.0$, and $\omega = 1.0$

	Melnikov Threshold values $(f_M^{\pm})$	
$\epsilon-$ values	f_M^-	f_M^+
0.1	0.17517	0.17517
0.17	0.29736	0.29736
0.2	0.17971	0.34977
0.3	0.44274	0.51077
0.4	0.46088	0.62415
0.5	0.46077	0.70023
0.6	0.46315	0.70805
0.7	0.44898	0.66667
0.8	0.44615	0.62302
0.9	0.45068	0.60714

5. CONCLUSION

The Melnikov method is sensitive to a global homoclinic bifurcation and gives a necessary condition for the occurrence of horseshoe chaos . Applying this method, we obtained the Melnikov threshold condition for onset of homoclinic transition to chaos that is transverse intersections of stable and unstable branches of homoclinic orbits. Threshold curves are drawn in a parameter space. These curves separating the chaotic and non-chaotic regions are obtained. Among the five periodic piecewise linear forces, f_M is maximum for the triangular type force. Also we have analyzed the occurrence of homoclinic transition to chaos in the Duffing system with an $\epsilon-$ parametric control force. The analytical results have been confirmed by numerical simulation. Numerical investigations including the computation of stable and unstable manifolds saddle and threshold curves are used to detect homoclinic transition to chaos. With the good agreement obtained between analytical and numerical predictions, we emphasize that the Melnikov analysis can be successfully used to predict the onset of chaos in the presence of weak periodic perturbation.

It is important to study the effect of nonlinear fractional damping in Duffing oscillator driven by periodic piecewise linear forces such as triangular, hat, trapezium, quadratic and rectangular types of forces. These will be investigated in future.

References

1. F.C. Moon and P.J. Holmes, A magnetoelastic strange attarctor, Journal of Sound and Vibration, 65, 1979, 275–296.
2. Y. Ueda and N. Akamatsu, Chaotically traditional phenomena in the forced negative-resistance oscillator, IEEE Transactions on Circuits and Systems, 28, 1981, 217–224.
3. C.S. Wang, Y.H. Kao, J.C. Huang and Y.S. Gou, Potential dependence of the bifurcation structure in generalized Duffing oscillators, Phys.Rev.E, 45, 1992, 3471–3485.
4. V. Ravichandran, V. Chinnathambi and S. Rajasekar, Effect of rectified and modulated sine forces on chaos in Duffing oscillator, Indian J. Phys., 83(11), 2009, 1593–1603.
5. V. Ravichandran, V. Chinnathambi and S. Rajasekar, Nonlinear resonance in Duffing oscillator with fixed and integrative time-delay feedback, Pramana Journal of Physics, 78, 2012, 347–360.
6. G. Chong, W. Hai and Q. Xei, Spatial chaos of trapped Bose-Einstein condensate in one-dimensional weak optical lattice potential, Chaos, 14, 2004, 217–223.
7. J. Heagy and W.L. Ditto, Dynamics of a two-frequency parametrically driven Duffing oscillator, J. of Nonlinear Science, 1, 1991, 423–455.
8. S. ValliPriyatharsini, M.V. Sethu Meenakshi, V. Chinnathambi and S. Rajasekar, Horseshoe dynamics in Duffing oscillator with fractional damping and multi-frequency excitation, Journal of Mathematical Modeling, 7(3), 2019, 263–276.
9. J. Guckenheimer and P. Holmes, Nonlinear Oscillations, Dynamical Systems and Bifurcations of Vector Fields, Springer-Verlag, New York, 1987.
10. M. Lakshmanan and S. Rajasekar, Nonlinear Dynamics, Integrability, Chaos and Patterns, Springer-Verlag, Berlin, 2003.
11. F.C. Moon, Chaotic Vibrations, An Introduction for Applied Scientists and Engineers, Wiley-Interscience, New York, 1987.
12. G. Litak, A. Siva and M. Borowiec, Homoclinic transition to chaos in the Ueda oscillator with external foring, arXiv:nlin/0610018v1[nlin.CD], 9-th Oct 2006.
13. E. Tyrkiel, On the role of chaotic saddles in generating chaotic dynamics in nonlinear driven oscillators, Int. J. Bifur. & Chaos, 15, 2005, 1215–1238.
14. L. Ravisankar, V. Ravichandran, V. Chinnathambi and S. Rajasekar, Nonlinear resonance in regular, random and small-world networks, Int. Journal of Physics, 7(1), 2014, 91–101.
15. B.K. Jones and G. Trefan, The Duffing oscillator: A precise electronic analog chaos demonstrator for the undergraduate laboratory, Am. J. Phys., 69(4), 2001, 464–469.
16. I.M. Kyprianidis, CH. Volos, I.N. Stouboulos and J. Hadjidemetriou, Dynamics of two resistively coupled Duffing-type electrical oscillators, Int. J. of Bifur. & Chaos, 16(6), 2006, 1765–1775.
17. V.K. Melnikov, On the stability of the center for time periodic perturbations, Trans. Moscow Math. Soc., 12(3), 1963, 1–57.
18. V. Ravichandran, S. Jeyakumari, V. Chinnathambi, S. Rajasekar and M.A.F. Sanjuan, Role of asymmetries on the chaotic dynamics of Double-well Duffing oscillator, Pramana Journal of Physics, 72, 2009, 927–937.
19. Z. Zing and J. Yang, Complex dynamics in pendulum equation with parametric and external perturbations, Int. J. of Bifur. & Chaos, 16(10), 2006, 3053–3078.

20. M.V. SethuMeenakshi, S. Athisayanathan, V. Chinnathambi and S. Rajasekar, Analytical estimates of the effect of amplitude modulated signal in nonlinearly damped Duffing-vander Pol oscillator, Chinese Journal of Physics, 55, 2017, 2208–2217.
21. M.V. Sethumeenakshi, S. Athisyanathan, V. Chinnathambi and S. Rajasekar, Effect of narrow band frequency modulated signal on horseshoe chaos in nonlinearly damped Duffing-vander Pol oscillator, Annual Review of Chaos, Theory, Bifurcations, and Dynamical Systems, 7, 2017, 41–55.
22. V. Ravichandran, V. Chinnathambi and S. Rajasekar, Homoclinic bifurcation and chaos in Duffing oscillator driven by an amplitude modulated force, Physica A, 376, 2007, 223–236.
23. B. Ravindra and A.K. Mallik, Role of nonlinear dissipation in soft Duffing oscillators, Phys. Rev. E., 49, 1994, 4950–4954.
24. M. Cai and J. Yang, Bifurcation of periodic orbits and chaos in Duffing equation, Acta Math. Appl. Sin, Engl. Ser., 22, 2006, 495- 508. https://doi.org/10.1007/s10255-006-0325-4
25. A.Y.T. Leung and Z. Liu, Suppressing chaos for some nonlinear oscillators, Int. J. of Bifur. & Chaos, 14(4), 2004, 1455–1465.
26. M.A.F. Sanjuan, The Effect of nonlinear damping on the universal escape oscillator, Int. J. Bifur. & Chaos, 9, 1999, 735–744.
27. A Sharma, V. Patidar, G. Purokit and K.K. Sud, Effects on the bifurcation and chaos in forced Duffing oscillator due to nonlinear damping, Commun. in Nonlinear Sci. and Numeri. Simulat., 176, 2012, 2254–2269.
28. M.V. Sethu Meenakshi, S. Athisayanathan, V. Chinnathambi and S. Rajasekar, Effct of fractional damping in double-well Duffing-vander Pol oscillator driven by different sinusoidal forces, Int. J. of Nonlinear Sci. and Numerical Simulation, 27(2), 2019, 81–94
29. R. Chacon, Control of homoclinic chaos by weak periodic perturbations, World Scientific, Singapore, 2005.
30. L. Ravisankar, V. Ravichandran and V. Chinnathambi, Prediction of horseshoe chaos in DVP oscillator driven by different periodic forces, Int. J. of Eng. and Sci., 1(5), 2012, 17–25.
31. Babar Ahmad, Stabilization of driven pendulum with periodic linear forces, Journal of Nonlinear Dynamics, Hindawi Publishing Corporation, 2013, Article ID: ID824701, 9 pages. http://dx.doi.org/10.1155/2013/824701, 2013.
32. S. Wiggins, Introduction to Applied Nonlinear Dynamical Systems and Chaos, Springer, New York, 1990.